





Topological pumping and Tamm states in photonic systemsSolange V. Silva ^{1,*}, David E. Fernandes ^{1,†}, Tiago A. Morgado ^{1,‡} and Mário G. Silveirinha ^{2,§}¹*Instituto de Telecomunicações and Department of Electrical Engineering, University of Coimbra, 3030-290 Coimbra, Portugal*²*University of Lisbon, Instituto Superior Técnico, Avenida Rovisco Pais, 1, 1049-001 Lisboa, Portugal*

(Received 9 December 2021; revised 8 March 2022; accepted 11 March 2022; published 19 April 2022)

The topology of typical Chern insulators is rooted in the periodicity of the system along two directions of real space. In this paper, we depart from this standard concept and demonstrate that a generic non-Hermitian photonic waveguide periodic along a single direction of real space can be regarded as a subcomponent of an extended system with a synthetic dimension and with a nontrivial Chern topology. We show that the number of bands below a bandgap of a generic waveguide determines the gap Chern number of the extended system. It is theoretically and numerically demonstrated that in real space the gap Chern number gives the number of gapless Tamm state branches localized at the system boundary, when its geometry is continuously displaced by one lattice period. In the non-Hermitian case, the Tamm states connect different bands in the complex plane.

DOI: [10.1103/PhysRevB.105.155133](https://doi.org/10.1103/PhysRevB.105.155133)**I. INTRODUCTION**

Topology has recently emerged as an indispensable tool to characterize global properties of physical systems, e.g., physical responses that are robust to perturbations of the system parameters [1–11]. There are different classes of topological platforms. Usually, a nontrivial topology is rooted in some particular symmetry or combination of symmetries of the system, e.g., invariance under discrete translations, time-reversal, or parity. For systems with a Chern-type classification, the topological analysis relies on the spectrum of some family of Hermitian operators $\hat{H}_{\mathbf{q}}$ parameterized by a two-component label $\mathbf{q} = (q_1, q_2)$ [12,13]. The Hermitian property is not essential [13–25]. Provided the two-parameter space is a closed surface with no boundary and $\hat{H}_{\mathbf{q}}$ varies smoothly with \mathbf{q} , then it is possible to assign a topological number C_{gap} to the spectral bandgaps. This result is known as the Chern theorem. The number C_{gap} is an integer, and its value is insensitive to perturbations of $\hat{H}_{\mathbf{q}}$ that do not close a bandgap.

In most studies so far, the topological properties are inherited from the periodicity of the system along two directions of real space, and \mathbf{q} is identified with a Bloch wave vector. The corresponding two-parameter space is a Brillouin zone, which is effectively a closed surface with no boundary (a torus) due to its cyclic nature. Here, we extend the Chern classification to generic one-dimensional (1D)-type photonic platforms, e.g., an arbitrary waveguide that supports propagation along a fixed direction of space. It is shown that any 1D-type periodic system can be regarded as a topological system with a synthetic dimension, and we theoretically and numerically demonstrate that the number of photonic bands below the gap is identical

to the gap Chern number. Furthermore, it is shown that edge states in the extended system with a synthetic dimension are mapped into Tamm states in the real space, i.e., to excitations localized at the end of the 1D photonic guide. In particular, it is demonstrated that the bulk-edge correspondence implies that the number of gapless Tamm states created when the geometry of the 1D periodic system is continuously displaced by one spatial period is determined by a difference of topological numbers. Finally, we demonstrate that the outlined ideas can be extended to non-Hermitian waveguides.

It should be noted that previous works [26–28] predicted topological light trapping on dislocations but using mechanisms different from ours. Furthermore, topological classifications of subclasses of 1D systems have been previously developed by other authors using Zak phases, winding numbers, and related concepts [28–32].

II. TOPOLOGICAL BAND COUNT

We consider a generic platform that is formed by a 1D real-space periodic system, which we shall designate as the *waveguide*. The waveguide can be visualized as some periodic [possibly three-dimensional (3D)] structure that only allows propagation (waveguiding) along some fixed direction, let us say the x direction. For example, it can be a hollow metallic structure, with the metal walls invariant to translations along the x axis, and with the guide periodically loaded with dielectric inclusions $\varepsilon(x, y, z) = \varepsilon(x + a, y, z)$; here, a is the lattice period. For simplicity, in most examples, we shall take the waveguide as a genuinely 1D photonic crystal formed by a periodic stack of dielectric slabs [$\varepsilon(x) = \varepsilon(x + a)$] and restrict our attention to propagation along the x axis. However, it is underlined that it can be fully 3D.

We admit that the wave propagation in the structure is determined by some operator $\hat{H}(\mathbf{r}, -i\nabla)$ such that the time evolution of the system state vector ψ , e.g., the electromagnetic field, is described by Schrödinger-type dynamics

*solange@co.it.pt

†dfernandes@co.it.pt

‡tiago.morgado@co.it.pt

§mario.silveirinha@co.it.pt

$i\partial_t\psi = \hat{H}\psi$. The time evolution of any (eventually dispersive) electromagnetic platform can always be expressed in such a manner [9,12,33,34]. For convenience, we designate \hat{H} as the Hamiltonian.

Due to the periodicity along the x direction, the eigenstates are Bloch waves labeled by a Bloch wave number q_x . The corresponding envelopes u_{q_x} (defined such that $\psi_{q_x} = u_{q_x}e^{iq_x x}$) satisfy $\hat{H}(x, -i\partial_x + q_x)u_{q_x} = \omega_{q_x}u_{q_x}$, with ω_{q_x} the eigenfrequencies. Note that u_{q_x} can be a multicomponent vector. The parameters $y, z, -i\partial_y,$ and $-i\partial_z$ are omitted from now on in the argument of the operator \hat{H} , as they are not relevant for the discussion.

Let us now add a second label (q_s) to the Hamiltonian related to a translation in space $x \rightarrow x - x_0$:

$$\hat{H}_{\mathbf{q}} \equiv \hat{H}_{q_x, q_s} = \hat{H}(x - x_0(q_s), -i\partial_x + q_x). \quad (1)$$

The coordinate shift x_0 is parameterized by q_s . In Sec. III, it will be shown that q_s may be understood as a *momentum* determined by a synthetic dimension. It is assumed that $x_0(q_s)$ is a smooth function and that $x_0(q_s + 2\pi) - x_0(q_s) = Na$, with a as the spatial period of the waveguide and N some integer number. Since $\hat{H}(x, -i\partial_x + q_x) = \hat{H}(x - a, -i\partial_x + q_x)$, it follows that \hat{H}_{q_x, q_s} is a periodic function of q_s with period 2π . In a full cycle, as q_s varies from $q_s = -\pi$ to $q_s = \pi$, the waveguide is displaced by N complete spatial periods toward the $+x$ direction.

Since the spectrum of \hat{H}_{q_x, q_s} is cyclic in both q_x and q_s , one can characterize its topological phases. To this end, consider a generic band of eigenfunctions ($\psi_{q_x}(x)$) of the waveguide: $\hat{H}(x, -i\partial_x)\psi_{q_x}(x) = \omega_{q_x}\psi_{q_x}(x)$. Then it is obvious that $\hat{H}_{\mathbf{q}}u_{\mathbf{q}} = \omega_{\mathbf{q}}u_{\mathbf{q}}$ with $\omega_{\mathbf{q}} = \omega_{q_x}$, $\mathbf{q} = (q_x, q_s)$, and with envelope given by

$$\begin{aligned} u_{\mathbf{q}}(x) &= \psi_{q_x}(x - x_0(q_s))e^{-iq_s x} \\ &= u_{q_x}(x - x_0(q_s))e^{-iq_s x_0(q_s)}. \end{aligned} \quad (2)$$

Clearly, the eigenvalues of $\hat{H}_{\mathbf{q}}$ are independent of q_s , and thereby, the bandgaps of $\hat{H}_{\mathbf{q}}$ are the same as the bandgaps of the waveguide. In other words, a translation in space does not alter the band structure.

In the following, it is assumed for simplicity that \hat{H} is a Hermitian operator. The generalization of the analysis to the non-Hermitian case is reported in Appendix A. The Bloch eigenmodes ψ_{q_x} of \hat{H} can be taken as smooth periodic functions of q_x in the 1D Brillouin zone $-\pi/a \leq q_x \leq \pi/a$. The Chern number \mathcal{C} associated with a given band of $\hat{H}_{\mathbf{q}}$ can be found in a standard way from the Berry potential $\mathcal{A}_{\mathbf{q}} = i\langle u_{\mathbf{q}} | \partial_{\mathbf{q}} u_{\mathbf{q}} \rangle$ using $\mathcal{C} = \frac{1}{2\pi} \int_{-\pi/a}^{\pi/a} dq_1 \int_{-\pi}^{\pi} dq_2 \left(\frac{\partial \mathcal{A}_{2, \mathbf{q}}}{\partial q_1} - \frac{\partial \mathcal{A}_{1, \mathbf{q}}}{\partial q_2} \right)$ with $(q_1, q_2) \equiv (q_x, q_s)$. The eigenfunctions are normalized as $\langle u_{\mathbf{q}} | u_{\mathbf{q}} \rangle = 1$, with $\langle \cdot | \cdot \rangle$ the canonical inner product. Since the Berry potential is a smooth function in the interior of the integration domain, from the Stokes theorem, the Chern number is

$$\begin{aligned} \mathcal{C} &= \frac{1}{2\pi} \int_{-\pi/a}^{\pi/a} dq_x (\mathcal{A}_{1, \mathbf{q}}|_{q_s=-\pi} - \mathcal{A}_{1, \mathbf{q}}|_{q_s=\pi}) \\ &+ \frac{1}{2\pi} \int_{-\pi}^{\pi} dq_s (\mathcal{A}_{2, \mathbf{q}}|_{q_x=\pi/a} - \mathcal{A}_{2, \mathbf{q}}|_{q_x=-\pi/a}). \end{aligned} \quad (3)$$

Using $u_{\mathbf{q}}(x) = \psi_{q_x}(x - x_0(q_s))e^{-iq_s x}$, one finds that $\mathcal{A}_{2, \mathbf{q}} = i\langle \psi_{\mathbf{q}} | \partial_{q_s} \psi_{\mathbf{q}} \rangle$ with $\psi_{\mathbf{q}} \equiv \psi_{q_x}(x - x_0(q_s))$. Noting that $i\langle \psi_{\mathbf{q}} | \partial_{q_s} \psi_{\mathbf{q}} \rangle$ is a periodic function of q_s , it follows that the second integral in the right-hand side of Eq. (3) vanishes. On the other hand, using $u_{\mathbf{q}}(x) = u_{q_x}(x - x_0(q_s))e^{-iq_s x_0(q_s)}$, we get

$$\mathcal{A}_{1, \mathbf{q}} = i\langle u_{q_x}(x - x_0(q_s)) | \partial_{q_x} [u_{q_x}(x - x_0(q_s))] \rangle + x_0(q_s). \quad (4)$$

We used $\langle u_{\mathbf{q}} | u_{\mathbf{q}} \rangle = 1$ and the periodicity of the envelope in x . The first term in the right-hand side of Eq. (4) is a periodic function of q_s because of the periodicity of the envelope in x . Thus, it does not contribute to the first integral in Eq. (3). Considering this, we obtain the key result:

$$\begin{aligned} \mathcal{C} &= \frac{1}{2\pi} \int_{-\pi/a}^{\pi/a} dq_x [x_0(-\pi) - x_0(\pi)] \\ &= -\frac{1}{a} [x_0(\pi) - x_0(-\pi)] = -N. \end{aligned} \quad (5)$$

We used $x_0(q_s + 2\pi) - x_0(q_s) = Na$ in the last identity. The above formula proves that each photonic band of $\hat{H}_{\mathbf{q}}$ has a topological charge of $-N$, i.e., identical to minus the number of displaced unit cells toward $+x$. Note that \mathcal{C} is an integer. In particular, the gap Chern number of a given bandgap is identical to the number of bands (n_{bands}) below the gap multiplied by the number of shifted cells (N) in one q_s cycle:

$$\mathcal{C}_{\text{gap}} = -n_{\text{bands}} \times N. \quad (6)$$

This means that the number of photonic bands below the gap of a generic 1D-type photonic crystal can be understood as a (topological) Chern number. The topological charge of each band is acquired from the translational shift suffered by the waveguide. In other words, a translation in space effectively pumps topological charge into the system described by $\hat{H}_{\mathbf{q}}$. This property and its consequences are discussed in Sec. III.

It is evident from the previous discussion that the topology of the operator $\hat{H}_{\mathbf{q}}$ is generically nontrivial (as it depends solely on the number of bands), independent of the time-reversal symmetry of the corresponding physical waveguide described by $\hat{H}(x, -i\partial_x)$. In fact, $\hat{H}_{\mathbf{q}}$ always has a broken time-reversal symmetry, even when $\hat{H}(x, -i\partial_x)$ describes a time-reversal-invariant system. To demonstrate this explicitly, we consider for simplicity a scalar problem so that the time-reversal operator can be identified with the complex conjugation operator. The waveguide is time-reversal invariant if $\hat{H}(x, -i\partial_x + q_x) = \hat{H}^*(x, -i\partial_x - q_x)$. Using $\hat{H}_{\mathbf{q}} = \hat{H}(x - x_0(q_s), -i\partial_x + q_x)$ [Eq. (1)], one readily finds that the operator defined in the synthetic space satisfies

$$\begin{aligned} \hat{H}_{-\mathbf{q}}^* &= [\hat{H}(x - x_0(-q_s), -i\partial_x - q_x)]^* \\ &= \hat{H}(x - x_0(-q_s), -i\partial_x + q_x) \neq \hat{H}_{\mathbf{q}}. \end{aligned} \quad (7)$$

In the second identity, we used the time-reversal invariance in real space. As seen, $\hat{H}_{-\mathbf{q}}^* \neq \hat{H}_{\mathbf{q}}$, and thereby, the system in the synthetic space always has a broken time-reversal symmetry, which can be attributed to the synthetic motion associated with the continuous translation in space described by $x_0(q_s)$.

III. THE SYNTHETIC DIMENSION AND BULK-EDGE CORRESPONDENCE

A. The synthetic dimension

Next, it is shown that \hat{H}_q can be regarded as the momentum-space operator of a system that consists of the original 1D-type waveguide (which, as previously mentioned, can be embedded in a 3D space) with an additional synthetic dimension. Systems with synthetic dimensions were recently discussed in the literature to emulate physical and topological phenomena in higher dimensions (see, e.g., Refs. [35–37]).

Consider a generic family of operators $\hat{H}_{\mathcal{K}}(x, -i\partial_x)$ periodic both in \mathcal{K} and x : $\hat{H}_{\mathcal{K}} = \hat{H}_{\mathcal{K}+2\pi}$ and $\hat{H}_{\mathcal{K}}(x, -i\partial_x) = \hat{H}_{\mathcal{K}}(x+a, -i\partial_x)$. The operator $\hat{H}_{\mathcal{K}}(x, -i\partial_x)$ may also depend on other space coordinates (y, z , etc.) and space derivatives, but since they are not relevant for the analysis, they are omitted. We introduce a matrix operator ($\hat{\mathcal{H}}_e$) that acts on a column state vector of the form $\Psi = [\psi_m(x)] = [\dots \psi_{-1} \ \psi_0 \ \psi_1 \ \dots]^T$, $m = 0, \pm 1, \pm 2, \dots$, through a convolution:

$$\Psi \rightarrow \hat{\mathcal{H}}_e \Psi = [(\hat{\mathcal{H}}_e \Psi)_n], \quad \text{where}$$

$$(\hat{\mathcal{H}}_e \Psi)_n = \sum_m \hat{H}_{n-m}(x, -i\partial_x) \psi_m(x), \quad (8)$$

with $n = 0, \pm 1, \pm 2, \dots$. The matrix elements of $\hat{\mathcal{H}}_e$ are defined as

$$\hat{H}_m(x, -i\partial_x) = \frac{1}{2\pi} \int_0^{2\pi} d\mathcal{K} \hat{H}_{\mathcal{K}}(x, -i\partial_x) e^{i\mathcal{K}m},$$

$$m = 0, \pm 1, \pm 2, \dots \quad (9)$$

The state vector $\Psi = [\psi_m(x)]$ has two space-type coordinates: x which corresponds to a continuous real-space coordinate and m which corresponds to a discrete (lattice) coordinate. The coordinate m determines the synthetic dimension. The Bloch eigenfunctions are characterized by a state vector of the form $\Psi = [\psi_m(x)]$, with $\psi_m(x) = u_{k,\mathcal{K}}(x) e^{ikx} e^{im\mathcal{K}}$, and satisfy $\hat{\mathcal{H}}_e \Psi = \omega_{k,\mathcal{K}} \Psi$, where (k, \mathcal{K}) is the two-dimensional (2D) Bloch wave vector ($-\pi/a \leq k \leq \pi/a$ and $-\pi \leq \mathcal{K} \leq \pi$). Substituting $\Psi = [u_{k,\mathcal{K}}(x) e^{ikx} e^{im\mathcal{K}}]$ into Eq. (8) and using the Fourier synthesis relation $\hat{H}_{\mathcal{K}}(x, -i\partial_x) = \sum_n \hat{H}_n(x, -i\partial_x) e^{-in\mathcal{K}}$, it is found that the secular equation $\hat{\mathcal{H}}_e \Psi = \omega_{k,\mathcal{K}} \Psi$ reduces to

$$\hat{H}_{\mathcal{K}}(x, -i\partial_x + k) u_{k,\mathcal{K}} = \omega_{k,\mathcal{K}} u_{k,\mathcal{K}}. \quad (10)$$

Thus, the operator $\hat{H}_{\mathcal{K}}(x, -i\partial_x + k)$ is the momentum-space version of $\hat{\mathcal{H}}_e$.

The previous theory can be readily applied to the family of operators $\hat{H}_q = \hat{H}(x - x_0(q_s), -i\partial_x + q_x)$ considered in Sec. II, with the obvious correspondence $(q_x, q_s) \leftrightarrow (k, \mathcal{K})$. Here, \hat{H}_q is the momentum-space version of some operator $\hat{\mathcal{H}}_e$ defined on an extended space determined by the continuous coordinate x (which varies in the real space) and by the discrete coordinate m (which varies along the synthetic lattice-type dimension). This property is important, as it guarantees that the gap Chern number can be linked to the number of edge states through a bulk-edge correspondence [13,38–42].

B. The bulk-edge correspondence

The bulk-edge correspondence establishes a precise relation between the gap Chern numbers of two topological materials and the net number of unidirectional edge states [38–44]. Thus, the Chern invariants of the operator $\hat{\mathcal{H}}_e$ determine a bulk-edge correspondence in the extended space with a synthetic dimension. An obvious question is: What are the consequences of the bulk-edge correspondence in real space?

To address this point, consider two 1D-type periodic waveguides, described by the (real-space) Hamiltonians \hat{H}_1 and \hat{H}_2 , respectively. Suppose that the waveguides have a common bandgap. Furthermore, let us add a synthetic (discrete) dimension to each waveguide, such that the extended-space Hamiltonians are $\hat{\mathcal{H}}_{e1}$ and $\hat{\mathcal{H}}_{e2}$, with each of them described by a momentum-space Hamiltonian of the form $\hat{H}_{q,i} = \hat{H}_i(x - x_0^{(i)}(q_s), -i\partial_x + q_x)$, $i = 1, 2$. For definiteness, we take $x_0^{(i)}(q_s) \equiv N_i \Delta$, with N_i an integer and $\Delta = \frac{q_s}{2\pi} a$. Then from Eq. (6), the gap Chern number difference in a common gap is

$$\delta \mathcal{C}_{\text{gap}} \equiv \mathcal{C}_{\text{gap},1} - \mathcal{C}_{\text{gap},2} = n_{\text{bands},2} \times N_2 - n_{\text{bands},1} \times N_1. \quad (11)$$

Here, $n_{\text{bands},i}$ is the number of bands below the gap for the i -th waveguide. In particular, when the number of shifted cells in both waveguides is $N_2 = N_1 = 1$, the gap Chern number difference is given by the difference of the number of bands below the gap, which thereby is a topological quantity.

The bulk-edge correspondence implies that an interface of the two topological platforms supports $|\delta \mathcal{C}_{\text{gap}}|$ unidirectional gapless edge states. A generic interface in the extended space does not have an obvious real-space geometric interpretation. The exceptions are the $x = \text{const.}$ interfaces, which correspond to standard real-space interfaces between the two waveguides. It is implicit that the waveguide cross-sections are identical when they are embedded in a 3D space.

Let us investigate the consequences of the bulk-edge correspondence for an interface $x = \text{const.}$, let us say $x = 0$. By definition, the edge states in the extended space must be localized near $x = 0$ and have a variation along the synthetic dimension (coordinate n) of the form e^{inq_s} , with q_s the wave number of the edge state in the synthetic dimension: $\Psi = [\psi_n(x)]$ with $\psi_n(x) = \psi(x) e^{inq_s}$ ($n = 0, \pm 1, \pm 2, \dots$). Evidently, the edge states projection into real space [$\psi_0(x) = \psi(x)$] corresponds to a wave trapped at the interface $x = 0$ of the two waveguides. A fixed q_s in extended space corresponds to a spatial shift $x_0^{(i)} = N_i \frac{q_s}{2\pi} a$ in real space. Thus, as q_s varies from 0 to 2π , the internal structure of the i -th waveguide is displaced by N_i cells. For some combinations of the shifts, the $x = 0$ interface can support trapped (localized) states, typically designated as Tamm states [45]. The bulk-edge correspondence establishes that the number of gapless Tamm states branches in real space is precisely $|\delta \mathcal{C}_{\text{gap}}|$, which is another key result of the paper.

C. Numerical examples

To illustrate the developed ideas, we consider the case where the waveguides are 1D photonic crystals formed by stacked dielectric slabs [see Fig. 1(a)(i) for the geometry of a generic binary photonic crystal]. All the materials are

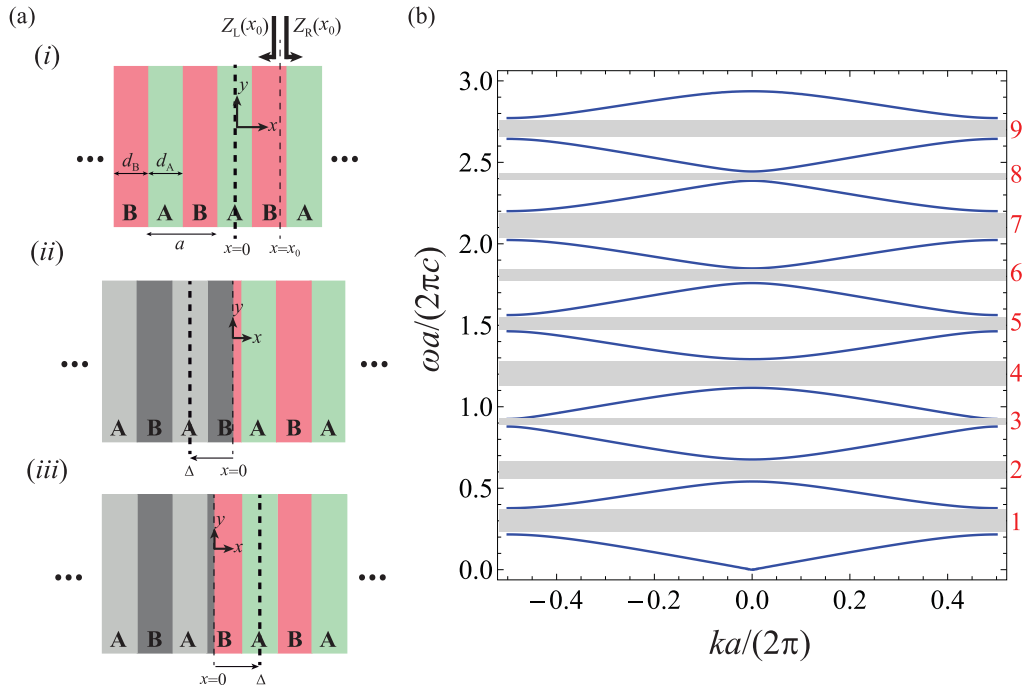


FIG. 1. (a) (i) Structure of a binary photonic crystal formed by two phases A and B. The left and right Bloch surface impedances calculated at the generic plane $x = x_0$ are indicated in the figure. The $x = 0$ plane is placed at the middle of slab A (center of symmetry). (ii) Representation of a negative displacement of the geometry of the photonic crystal. (iii) Representation of a positive displacement of the geometry. The areas shaded in gray are cut away from the structure when another photonic crystal is inserted into the region $x < 0$. (b) Band structure of a photonic crystal (blue solid curves) with parameters $\varepsilon_A = 7$, $\varepsilon_B = 1$, $d_A = 0.4a$, and $d_B = 0.6a$. The gray strips represent the bandgaps. Each bandgap is numbered with a red label.

nonmagnetic ($\mu = \mu_0$). The band structure of a 1D photonic crystal can be calculated with standard methods [46]. We denote $Z_L(x_0, \omega)$ and $Z_R(x_0, \omega)$ as the Bloch impedances of the (unbounded) photonic crystal calculated at the plane $x = x_0$ when looking at the left or right, respectively [Fig. 1(a)(i)]. The band diagram and the Bloch impedances are numerically evaluated as explained in Appendix B.

Consider the scenario where two photonic crystals are paired to form an interface at $x = 0$ [Fig. 2(a)(i)]. The semispace $x < 0$ is filled with a photonic crystal modeled by $\hat{H}_1(x - x_0^{(1)}(q_s), -i\partial_x)$, and the semispace $x > 0$ by a photonic crystal modeled by $\hat{H}_2(x - x_0^{(2)}(q_s), -i\partial_x)$, with $x_0^{(i)} = N_i\Delta$. The trapped (defect-type) states at $x = 0$ are the solutions of the characteristic equation [28]:

$$Z_L^{(1)}(-N_1\Delta, \omega) + Z_R^{(2)}(-N_2\Delta, \omega) = 0. \quad (12)$$

Here, $Z_L^{(i)}$ and $Z_R^{(i)}$ are the left and right Bloch impedances of the i -th photonic crystal. Each value of $\Delta = \frac{q_s}{2\pi}a$ corresponds to a specific spatial shift of the inner structure of the photonic crystals. In one full q_s cycle, the parameter Δ varies from $\Delta = 0$ to $\Delta = a$. The effect of shifting the geometry of a generic photonic crystal is illustrated in Figs. 1(a)(ii) and 1(a)(iii).

In the first example, we suppose that the semispace $x < 0$ is a perfectly electric conducting (PEC) wall, so that $Z_L^{(1)} = 0$. The semispace $x > 0$ is filled with a binary photonic crystal with a unit cell formed by two dielectric slabs A and B of thickness d_A and d_B and relative dielectric permittivity ε_A and ε_B , respectively [see Fig. 1(a)]. The structural param-

eters are taken as $\varepsilon_A = 7$, $\varepsilon_B = 1$, $d_A = 0.4a$, and $d_B = 0.6a$. Figure 1(b) shows the numerically calculated band structure (ω vs $k \equiv q_x$) with the bandgaps shaded in gray. Since for the PEC semispace $\mathcal{C}_{\text{gap},1} = 0$, it follows that the gap Chern number difference is $\delta\mathcal{C}_{\text{gap}} = n_{\text{bands},2} \times N_2$ [Eq. (11)]. Interestingly, the gap Chern number of the dielectric photonic crystal with the synthetic dimension is nonzero, even though the structure in real space is reciprocal. In typical systems, reciprocity (time-reversal symmetry) implies a trivial Chern topology [4]. In contrast, in our problem, the time-reversal symmetry in real space does not imply the time-reversal symmetry in the extended space, as already discussed in the end of Sec. II.

Suppose that $N_2 = -1$, so that the photonic crystal is displaced by a complete period to the negative x axis in a full Δ cycle [Fig. 1(a)(ii)]. The dispersion of the interface states as a function of the spatial shift Δ is determined from $Z_R^{(2)}(\Delta, \omega) = 0$. The corresponding solutions in the bandgaps are plotted in Fig. 2(b) (blue curves). As seen, in agreement with the bulk-edge correspondence, $\delta\mathcal{C}_{\text{gap}} = -n_{\text{bands},2}$, the number of branches $\omega = \omega_n(\Delta)$ in each gap is exactly coincident with the number of bands below the gap. Each branch $\omega_n(\Delta)$ completely crosses the bandgap, and all the branches have a positive slope vs Δ , indicating that they are unidirectional gapless states in the extended space with the synthetic dimension. Our formalism enables us to predict in a simple way how many (defect-type) trapped states occur in real space for a fixed frequency in the bandgap when the geometry of the crystal is displaced by one period. The number of Tamm state

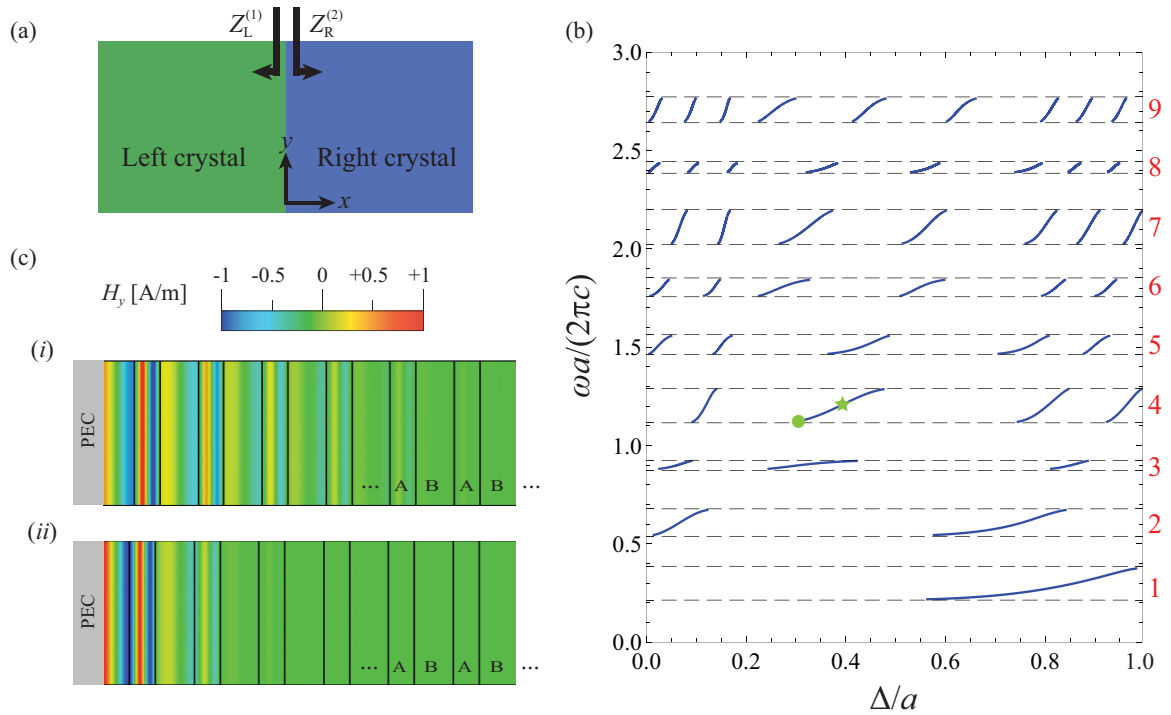


FIG. 2. (a) Representation of the pairing of two different photonic crystals. (b) Interface state solutions for a photonic crystal with the same parameters as in Fig. 1(b) in the right semispace, and a perfectly electric conducting (PEC) material in the left semispace. The gray horizontal dashed lines delimit the bandgaps which are numbered by the red labels. (c) Time snapshot of the magnetic field of the interface state in the fourth gap for (i) the solution marked by the green circle with $\Delta/a = 0.3$, and (ii) the solution marked by the green star with $\Delta/a = 0.38$.

branches is exactly the number of bands below the gap, i.e., it equals the topological invariant. The operation of a spatial shift by one period may be regarded as a *topological pump* that inserts topological charge into the system, with the topological charge identical to the number of bands below the gap. The topological protection of the gapless states implies that any perturbation of the bulk photonic crystal in real space that does not close the relevant bandgap will always produce the same number of Tamm state branches.

The profile of two trapped states in the fourth bandgap is represented in Fig. 2(c). The field profiles were obtained using CST Studio Suite [47]. As seen, the trapped states are confined to the boundary of the photonic crystal and decay exponentially into the bulk region. As could be expected, the trapped mode in the center of the bandgap [Fig. 2(c)(ii) for $\Delta = 0.38$] is much more confined to the interface than the one near the bottom edge of the bandgap [Fig. 2(c)(i) for $\Delta = 0.30$]. It is underlined that the Tamm states in the real physical space are bound states attached to the interface and are not associated with a flow of energy. In contrast, in the synthetic space, they transport energy and are associated with the synthetic momentum $q_s = 2\pi\Delta/a$.

In the second example, the PEC region in the semispace $x < 0$ is replaced by a binary photonic crystal with parameters $\varepsilon_{A,1} = 2$, $\varepsilon_{B,1} = 1$, $d_{A,1} = 0.4a$, and $d_{B,1} = 0.6a$, with the photonic crystal in the semispace $x > 0$ the same as before. Figure 3(a) shows the band structures of the right (blue solid curve) and left (green dashed curve) crystals. There are two common frequency bandgaps highlighted with the shaded gray strips. Consider first the situation wherein

one of the photonic crystals is held fixed, while the other crystal is displaced by one cell period to the negative x direction.

Figure 3(b) depicts the interface states dispersion $\omega = \omega_n(\Delta)$ in the two common gaps for the two possible displacements: (i) the left crystal is held fixed, and the right crystal slides to the left [blue solid curves; $N_1 = 0$ and $N_2 = -1$ in Eq. (12)], (ii) the right crystal is held fixed, and the left crystal slides to the left [green dashed curves; $N_1 = -1$ and $N_2 = 0$ in Eq. (12)]. For the case (i) [case (ii)], the number of solution branches is identical to the number of bands of the right (left) crystal below the gap, consistent with the bulk-edge correspondence [see Eq. (11)]. The slope of the curves $\omega = \omega_n(\Delta)$ is different in the two cases. This property is explained by the fact that $\delta\mathcal{C}_{\text{gap}}$ has a different sign in each case. Indeed, the sign of $\delta\mathcal{C}_{\text{gap}}$ is linked to the angular momentum of the edge modes in a closed system [42,48,49]. Thereby, the direction of the energy flow in the extended space must change when the gap Chern number sign changes.

We also studied the situations where the photonic crystals are simultaneously displaced to the negative x direction $N_1 = N_2 = -1$ [blue solid curves in Fig. 3(c)], or alternatively, the right crystal is displaced to the negative x direction and the left crystal to the positive x direction ($N_1 = 1$ and $N_2 = -1$) [green dashed curves in Fig. 3(c)]. In both cases, it is observed that the number of trapped state branches in a common bandgap is identical to $|\delta\mathcal{C}_{\text{gap}}| \equiv |n_{\text{bands},2} \times N_2 - n_{\text{bands},1} \times N_1|$. For example, for the lowest frequency gap $n_{\text{bands},2} = 4$ and $n_{\text{bands},1} = 3$. Consistent with this property, there is a single gapless trapped state

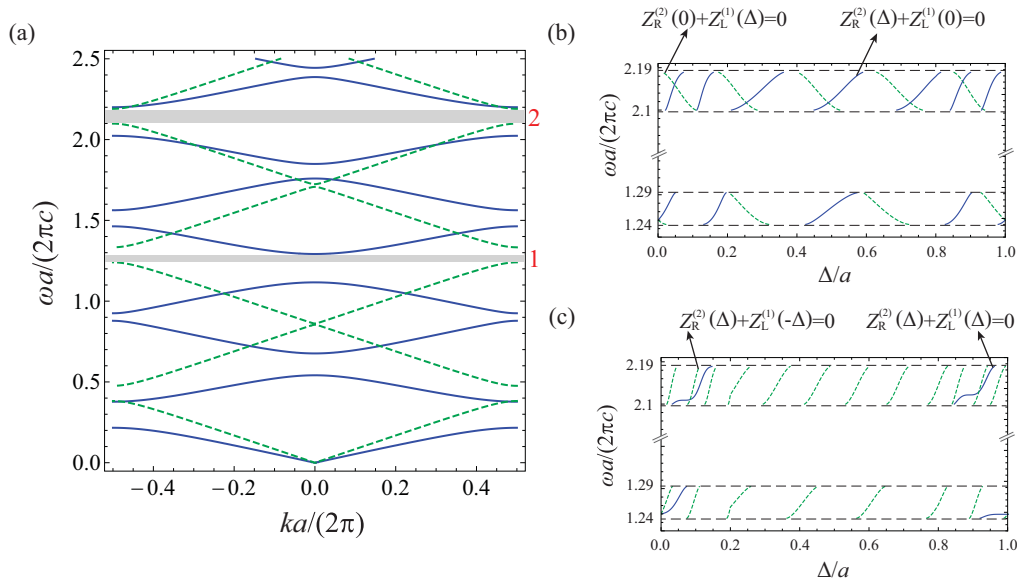


FIG. 3. (a) Green dashed curves: band structure of a binary photonic crystal with parameters $\epsilon_{A,1} = 2$, $\epsilon_{B,1} = 1$, $d_{A,1} = 0.4a$, and $d_{B,1} = 0.6a$. Blue solid curves: band structure of the same photonic crystal as in Fig. 1. The gray strips indicate the common bandgaps and the red labels the gap number. (b) Dispersion of the interface states in the common bandgaps for a negative displacement of one of the crystals with the other held fixed. Blue solid curves: right photonic crystal slides one cell to the left; green dashed curves: left photonic crystal slides one cell to the left. (c) Similar to (b) but for a situation where both crystals suffer a negative spatial shift (blue solid curves, $N_1 = N_2 = -1$), or alternatively, the left crystal suffers a positive spatial shift and the right crystal a negative spatial shift (green dashed curves, $N_1 = 1$ and $N_2 = -1$).

branch when $N_1 = N_2 = -1$ and seven gapless trapped states branches when $N_1 = -N_2 = 1$.

We verified that the bulk-edge correspondence also holds true for other more complex 1D photonic crystal geometries. For example, suppose that the left photonic crystal of the previous example is replaced by a ternary layered structure with parameters $\epsilon_{A,1} = 2$, $\epsilon_{B,1} = 1$, $\epsilon_{C,1} = 3$, $d_{A,1} = 0.3a$, $d_{B,1} = 0.6a$, and $d_{C,1} = 0.1a$. Different from the binary crystals con-

sidered in the previous examples, the ternary crystal does not have inversion (parity) symmetry. Figure 4 reports a study identical to that of Fig. 3, when the ternary photonic crystal (region $x < 0$) is paired with the same binary photonic crystal as in Fig. 2. The results are qualitatively analogous to those of Fig. 3 and again confirm that it is possible to predict the number of Tamm states from the knowledge of the number of bands below the bandgap. Curiously, in this example, the

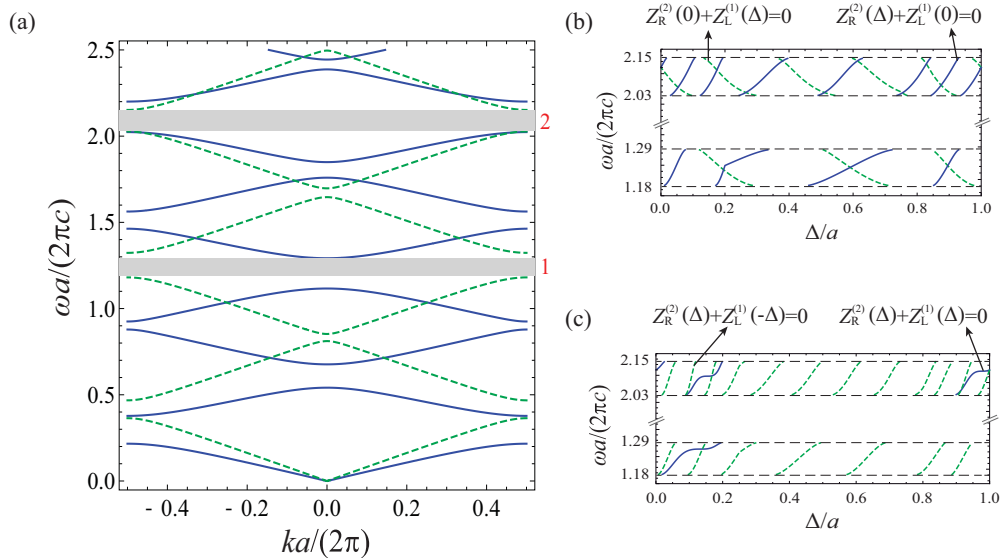


FIG. 4. Analogous to Fig. 3(a) for the case where the photonic crystal in the semispace $x < 0$ is replaced by a ternary photonic crystal with parameters $\epsilon_{A,1} = 2$, $\epsilon_{B,1} = 1$, $\epsilon_{C,1} = 3$, $d_{A,1} = 0.3a$, $d_{B,1} = 0.6a$, and $d_{C,1} = 0.1a$. The band structure of the ternary photonic crystal is represented with green dashed curves in (a).

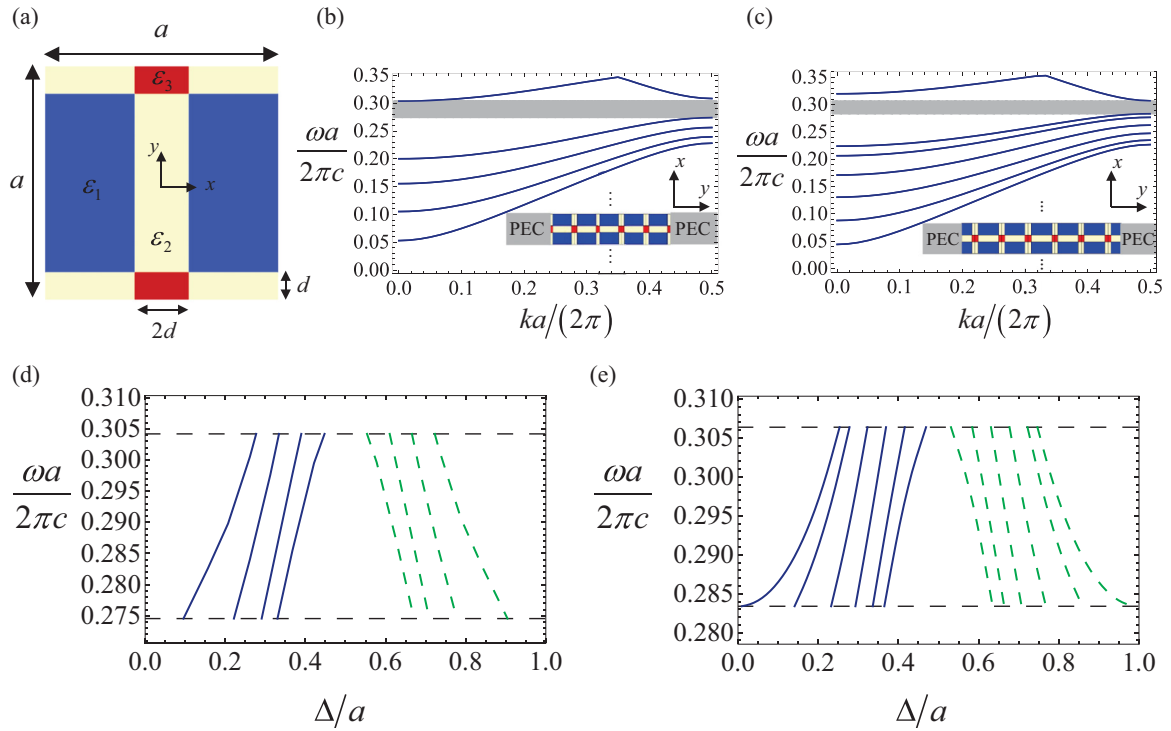


FIG. 5. (a) Unit cell of a two-dimensional (2D) photonic crystal with $\epsilon_1 = 1$, $\epsilon_2 = 6.5$, and $\epsilon_3 = 12$. The unit cell period is a . The parameter d represented in the figure is $d = 0.115a$. (b) Band diagram of the waveguide with metallic lateral walls constructed from a 2D photonic crystal with 5 unit cells along the y direction. The shaded gray strip indicates the bandgap of the waveguide. (c) Similar to (b) but for a waveguide constructed from a 2D photonic crystal with 6 unit cells along the y direction. (d) Dispersion of the interface states in the bandgap for a waveguide constructed from a 2D photonic crystal with 5 unit cells along the y direction, placed in the semispace $x > 0$ and terminated with a metallic plate placed at $x = 0$. The waveguide geometry is continuously displaced by one lattice period along the x direction. Blue solid curves: negative displacement ($N_2 = -1$). Green dashed curves: positive displacement ($N_2 = 1$). (e) Similar to (d) but for a waveguide constructed from a 2D photonic crystal with 6 unit cells along the y direction.

slope of the trapped state dispersion can be discontinuous [see the low-frequency gap in Fig. 4(b), blue lines]. This feature is due to the discontinuity of the permittivity profile of the photonic crystals.

Furthermore, we also studied the emergence of interface states in 1D-type waveguides embedded in a 2D real space. Specifically, consider a waveguide with metallic lateral walls constructed from a 2D photonic crystal with the unit cell represented in Fig. 5(a). The lateral width of the guide is $N_y a$, and the electric field is oriented along the z direction. The corresponding band diagram for propagation along the x direction is represented in Figs. 5(b) and 5(c) for the cases $N_y = 5$ and 6, respectively. The band diagram is numerically calculated with CST Studio Suite [47]. The bandgaps are shaded in gray. We terminated this waveguide (positioned in the semispace $x > 0$) with a metallic plate placed at $x = 0$ and numerically found the edge states for different shifts of the waveguide geometry. The trapped state dispersion $\omega = \omega_n(\Delta)$ is shown in Figs. 5(d) and 5(e). We consider displacements along the negative ($N_2 = -1$, blue curves) and positive ($N_2 = 1$, green dashed curves) x axis. As seen, also for this more complex system, the number of branches agrees with the number of bands of the waveguide below the gap. Furthermore, as expected, the slope of the curves $\omega = \omega_n(\Delta)$ depends on the displacement direction.

Finally, we present an example of a non-Hermitian photonic crystal. Topological effects in non-Hermitian systems have received great attention in recent years [13–25]. For simplicity, the material dispersion is ignored here. The geometry of the photonic crystals is as in Fig. 1, except that the permittivity of the material A is taken equal to $\epsilon_A = 7 + 0.1i$, so that the photonic crystal is lossy. We calculated the complex band structure of the photonic crystal $\omega(q_x) = \omega' + i\omega''$ using the plane-wave method [46]. Figure 6 shows a parametric plot of $\omega(q_x)$ in the complex plane with $-\pi/a < q_x < \pi/a$, i.e., the figure represents the projected band structure. As seen, the projected band structure is formed by disconnected regions (blue curves). Each disconnected region corresponds to a bulk band [13]. We determined the dispersion of the (complex) Tamm states when the photonic crystal is paired with a PEC wall. To this end, we solved $Z_R^{(2)}(\Delta, \omega) = 0$ for $\Delta = \frac{q_s}{2\pi} a$ real valued ($N_2 = -1$). The green lines in Fig. 6 represent a parametric plot of the dispersion of the Tamm states $\omega(q_s)$ in the complex plane. In agreement with the bulk-edge correspondence, the number of Tamm state branches (in green) in each gap is identical to the number of bulk bands (in blue) on the left of the gap. The Tamm states link the different bulk bands and thereby are gapless. These properties confirm the topological nature of the Tamm states supported by non-Hermitian photonic crystals. Both the bulk bands and

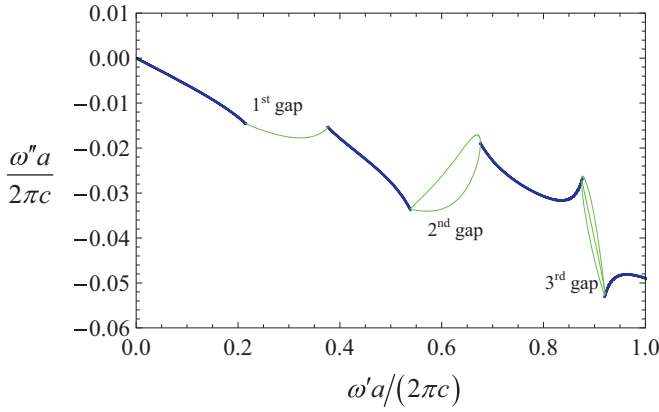


FIG. 6. Projected band structure $\omega = \omega' + i\omega''$ of a non-Hermitian photonic crystal with parameters $\varepsilon_A = 7 + 0.1i$, $\varepsilon_B = 1$, $d_A = 0.4a$, and $d_B = 0.6a$. The blue solid curves represent the different bulk bands. The green curves represent the projected dispersion of the edge states (Tamm states) of the extended synthetic system. The edge modes are gapless, as they connect different bands. The number of Tamm states branches in a gap is identical to the gap number.

the edge state modes have an oscillation frequency such that $\omega'' = \text{Im}\{\omega\} < 0$ because of loss.

IV. CONCLUSIONS

In summary, it was shown that in 1D periodic systems the number of bands below a gap can be understood as a Chern topological number of an extended system with a synthetic dimension. This topological number determines the number of edge states in the extended space with the synthetic dimension. The real-space projection of the edge states are modes localized at the boundary of the 1D crystal (Tamm states) for some shift of the unit cell. The number of Tamm state branches “pumped” by a full-lattice period displacement equals the number of bands below the gap. This result is not rooted in any particular symmetry and is valid for non-Hermitian operators. Thereby, in this paper, we establish a rigorous and simple bulk-edge correspondence for 1D systems and uncover a different topological mechanism to localize light at an interface of two arbitrary photonic waveguides.

ACKNOWLEDGMENTS

This paper was partially funded by the Institution of Engineering and Technology, by the Simons Foundation, and by Instituto de Telecomunicações under Project No. UID/EEA/50008/2020. S.V.S. acknowledges financial support by Fundação para a Ciência e a Tecnologia (FCT/POPH) and the cofinancing of Fundo Social Europeu under the Ph.D. fellowship SFRH/BD/105625/2015. D.E.F. acknowledges support by FCT, POCH, and the cofinancing of Fundo Social Europeu under the fellowship SFRH/BPD/116525/2016. T.A.M. acknowledges FCT for research financial support with reference CEECIND/04530/2017 under the CEEC (Concurso Estímulo ao Emprego Científico) Individual 2017, and IT-Coimbra for the contract as an assistant researcher with reference CT/No. 004/2019-F00069.

APPENDIX A: CALCULATION OF THE CHERN NUMBER FOR A NON-HERMITIAN SYSTEM

In this Appendix, we extend the theory of Sec. II to non-Hermitian operators \hat{H} . In such a case, the Berry connection must be defined using both the left and right eigenvectors of \hat{H} [13,19]. If the operator \hat{H} is diagonalizable, it is possible to pick the left and right eigenvectors such that $\langle u_{q_x,n}^L | u_{q_x,m}^R \rangle = \delta_{nm}$, where the indices n and m identify different photonic bands. Here, $u_{q_x,m}^R$, $u_{q_x,n}^L$ are the envelopes of the Bloch eigenmodes $[\psi_{q_x,m}^R(x)$ and $\psi_{q_x,n}^L(x)]$ of the operators \hat{H} and \hat{H}^\dagger , respectively [13,19]. Typically, \hat{H} describes a system with material loss, whereas \hat{H}^\dagger describes the corresponding time-reversal symmetric system with material gain. In the following, it is assumed that $\psi_{q_x,m}^R(x)$ and $\psi_{q_x,n}^L(x)$ are periodic functions of q_x .

We denote $\hat{H}_q^R = \hat{H}_q$ and $\hat{H}_q^L = \hat{H}_q^\dagger$ as the right and left Hamiltonians of the system with the synthetic dimension obtained from \hat{H} and \hat{H}^\dagger using the same procedure as in the main text. Let us compute the Chern number associated with a generic (isolated) photonic band of the extended system. The Berry connection is defined by $\mathcal{A}_q = i\langle u_q^L | \partial_q u_q^R \rangle$ (the band index is dropped here) [13,19], with

$$\begin{aligned} u_q^i(x) &= \psi_{q_x}^i(x - x_0(q_s))e^{-iq_x x} \\ &= u_{q_x}^i(x - x_0(q_s))e^{-iq_x x_0(q_s)}, \quad i = L, R, \end{aligned} \quad (\text{A1})$$

and $\psi_{q_x}^R(x)$ and $\psi_{q_x}^L(x)$ the relevant Bloch eigenmodes of the 1D operators \hat{H} and \hat{H}^\dagger , respectively. Using the same arguments as in the main text, it is readily seen that the Chern number is still given by Eq. (3). Furthermore, now the second component of the Berry potential is $\mathcal{A}_{2,q} = i\langle \psi_q^L | \partial_{q_s} \psi_q^R \rangle$, which is evidently a periodic function of q_x . Hence, similar to the main text, it is found that

$$C = \frac{1}{2\pi} \int_{-\pi/a}^{\pi/a} dq_x (\mathcal{A}_{1,q}|_{q_s=-\pi} - \mathcal{A}_{1,q}|_{q_s=\pi}). \quad (\text{A2})$$

Using $u_q^i(x) = u_{q_x}^i(x - x_0(q_s))e^{-iq_x x_0(q_s)}$ [Eq. (A1)] and $\langle u_{q_x}^L | u_{q_x}^R \rangle = 1$, one readily finds that $\mathcal{A}_{1,q} = i\langle u_{q_x}^L(x - x_0(q_s)) | \partial_{q_x} [u_{q_x}^R(x - x_0(q_s))] \rangle + x_0(q_s)$. The first term of $\mathcal{A}_{1,q}$ is a periodic function of the synthetic momentum q_s , and thereby, the result of the main text [Eq. (5)] remains valid in the non-Hermitian case.

APPENDIX B: DISPERSION EQUATION AND BLOCH IMPEDANCE OF A 1D PHOTONIC CRYSTAL

Here, we derive the characteristic equation for the Bloch waves of a 1D layered photonic crystal and the Bloch wave impedances. The unit cell is formed by an arbitrary number (N) of layers (see Fig. 7 for the case $N = 3$).

As is well known, the wave propagation in a 1D photonic crystal is formally equivalent to the propagation in a periodic transmission line (Fig. 7). Thus, the characteristic equation for the Bloch waves can be easily found using the ABCD matrix formalism [50]. To this end, one needs to find the ABCD matrix for a unit cell, which links the input and output voltages

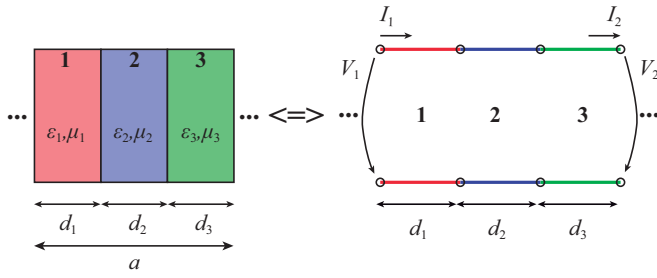


FIG. 7. Equivalence between a multilayered photonic crystal and a periodic transmission line.

and currents as

$$\begin{pmatrix} V_1 \\ I_1 \end{pmatrix} = \begin{pmatrix} A & B \\ C & D \end{pmatrix}_{\text{global}} \begin{pmatrix} V_2 \\ I_2 \end{pmatrix}. \quad (\text{B1})$$

From the theory of microwave networks, the global ABCD matrix is given by the product of the ABCD matrices of the uniform line sections:

$$\mathbf{M} \equiv \begin{pmatrix} A & B \\ C & D \end{pmatrix}_{\text{global}} = \begin{pmatrix} A & B \\ C & D \end{pmatrix}_1 \cdots \begin{pmatrix} A & B \\ C & D \end{pmatrix}_N. \quad (\text{B2})$$

In the above,

$$\begin{pmatrix} A & B \\ C & D \end{pmatrix}_i = \begin{bmatrix} \cosh(\gamma_i d_i) & Z_{c,i} \sinh(\gamma_i d_i) \\ Z_{c,i}^{-1} \sinh(\gamma_i d_i) & \cosh(\gamma_i d_i) \end{bmatrix}, \quad (\text{B3})$$

$$i = 1, 2, \dots, N,$$

is the ABCD matrix of the i th section, $Z_{c,i} = \eta_0 \sqrt{\mu_i/\epsilon_i}$ is the wave impedance, and $\gamma_i = -i \frac{\omega}{c} \sqrt{\mu_i \epsilon_i}$ is the propagation constant. Here, η_0 is the free-space impedance, and c is the speed of light in vacuum. The permittivity and permeability ϵ_i, μ_i are normalized to the free-space values.

For Bloch waves, the input and output voltages are linked by $\begin{pmatrix} V_2 \\ I_2 \end{pmatrix} = e^{-\gamma a} \begin{pmatrix} V_1 \\ I_1 \end{pmatrix}$, with $\gamma = \alpha - ik$ as the (complex) propagation constant of the Bloch mode. Thus, using Eq. (B1), one finds that the output voltages and currents satisfy the homogeneous equation:

$$(\mathbf{M} - \mathbf{1}e^{+\gamma a}) \cdot \begin{pmatrix} V_2 \\ I_2 \end{pmatrix} = 0, \quad (\text{B4})$$

with \mathbf{M} as the global ABCD matrix, as defined in Eq. (B2). This result implies that $\det(\mathbf{M} - \mathbf{1}\lambda) = 0$, or equivalently, $\lambda^2 - \lambda \text{tr}(\mathbf{M}) + \det(\mathbf{M}) = 0$, with $\lambda = e^{+\gamma a}$. Since the system under analysis is reciprocal, one has $\det(\mathbf{M}) = 1$ [50]. The solutions of the second-degree equation are $\lambda_{1,2} = \frac{\text{tr}(\mathbf{M})}{2} \pm \sqrt{\left[\frac{\text{tr}(\mathbf{M})}{2}\right]^2 - 1}$. Because of $\lambda_{1,2} = e^{\pm\gamma a}$, one has $e^{+\gamma a} + e^{-\gamma a} = \lambda_1 + \lambda_2 = \text{tr}(\mathbf{M})$. This implies that the characteristic equation for the Bloch waves is

$$\cosh(\gamma a) = \frac{\text{tr}(\mathbf{M})}{2}. \quad (\text{B5})$$

The photonic band structure of a Hermitian crystal is found by looking for solutions of the above equation with $\gamma = -ik$ as a purely imaginary number.

Next, we derive the formulas of the Bloch impedances $Z_L(x_0, \omega)$ and $Z_R(x_0, \omega)$. Let us suppose without loss of

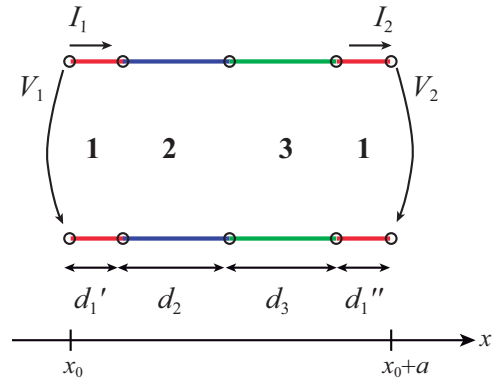


FIG. 8. Geometry used in the calculation of the Bloch impedance.

generality that $x = x_0$ lies in the first line section, as illustrated in Fig. 8.

It is useful to obtain the global ABCD matrix $[\mathbf{M}(x_0)]$ for one period, with the input and output voltages and currents referred to the planes $x = x_0$ and $x = x_0 + a$, respectively (Fig. 8). This is done as before by multiplying the ABCD matrices of the uniform line sections. For the example, for the geometry shown in Fig. 8, one has

$$\mathbf{M}(x_0) = \begin{pmatrix} A & B \\ C & D \end{pmatrix}_{1,d_1'} \begin{pmatrix} A & B \\ C & D \end{pmatrix}_{2,d_2} \begin{pmatrix} A & B \\ C & D \end{pmatrix}_{3,d_3} \begin{pmatrix} A & B \\ C & D \end{pmatrix}_{1,d_1''}. \quad (\text{B6})$$

Note that d_1' and d_1'' depend on x_0 . Similar to Eq. (B4), for Bloch waves associated with a propagation factor $e^{-(\pm\gamma)x}$, the output voltage and current satisfy

$$(\mathbf{M}(x_0) - \mathbf{1}e^{\pm\gamma a}) \cdot \begin{pmatrix} V_2 \\ I_2 \end{pmatrix} = 0. \quad (\text{B7})$$

Note that $\gamma = \gamma(\omega)$ depends exclusively on the frequency and can be found from Eq. (B5). In the bandgaps, γ is complex valued, and it is implicit that $\text{Re}\{\gamma\} > 0$. Denoting $\mathbf{M}(x_0) = \begin{pmatrix} A & B \\ C & D \end{pmatrix}$ it follows from Eq. (B7) that

$$\begin{pmatrix} V_2 \\ I_2 \end{pmatrix} \sim \begin{pmatrix} -B \\ A - e^{\pm\gamma a} \end{pmatrix} \sim \begin{pmatrix} D - e^{\pm\gamma a} \\ -C \end{pmatrix}. \quad (\text{B8})$$

Hence, the Bloch impedance for a wave that propagates toward the positive x direction is

$$Z_R(x_0) = \frac{V_2}{I_2} = \frac{-B}{A - e^{\gamma a}} = \frac{D - e^{\gamma a}}{-C}, \quad (\text{B9a})$$

whereas the Bloch impedance for a wave that propagates toward the negative x direction is

$$Z_L(x_0) = \frac{V_2}{-I_2} = \frac{B}{A - e^{-\gamma a}} = \frac{D - e^{-\gamma a}}{C}. \quad (\text{B9b})$$

We used the fact that the Bloch impedances are periodic: $Z_R(x_0) = Z_R(x_0 + a)$, etc.

The trapped states at an interface ($x = 0$) between two semi-infinite photonic crystals are forcibly decaying in space Bloch modes of the infinite photonic crystals in the regions $x > 0$ and $x < 0$. Thereby, since the current and voltage are continuous at the interface $x = 0$, the localized trapped states must satisfy $Z_L^{(1)}(x = 0, \omega) + Z_R^{(2)}(x = 0, \omega) = 0$, consistent with the main text.

- [1] M. Z. Hasan and C. L. Kane, Colloquium: Topological insulators, *Rev. Mod. Phys.* **82**, 3045 (2010).
- [2] X. L. Qi and S. C. Zhang, Topological insulators and superconductors, *Rev. Mod. Phys.* **83**, 1057 (2011).
- [3] F. D. M. Haldane, Nobel lecture: Topological quantum matter, *Rev. Mod. Phys.* **89**, 040502 (2017).
- [4] F. D. M. Haldane and S. Raghunathan, Possible Realization of Directional Optical Waveguides in Photonic Crystals with Broken Time-Reversal Symmetry, *Phys. Rev. Lett.* **100**, 013904 (2008).
- [5] Z. Wang, Y. Chong, J. D. Joannopoulos, and M. Soljačić, Observation of unidirectional backscattering immune topological electromagnetic states, *Nature (London)* **461**, 772 (2009).
- [6] A. B. Khanikaev, S. H. Mousavi, W. K. Tse, M. Kargarian, A. H. MacDonald, and G. Shvets, Photonic topological insulators, *Nat. Mater.* **12**, 233 (2012).
- [7] M. C. Rechtsman, J. M. Zeuner, Y. Plotnik, Y. Lumer, D. Podolsky, F. Dreisow, S. Nolte, M. Segev, and A. Szameit, Photonic Floquet topological insulators, *Nature* **496**, 196 (2013).
- [8] L. Lu, J. D. Joannopoulos, and M. Soljačić, Topological photonics, *Nat. Photonics* **8**, 821 (2014).
- [9] M. G. Silveirinha, Chern invariants for continuous media, *Phys. Rev. B* **92**, 125153 (2015).
- [10] S. A. H. Gangaraj, M. G. Silveirinha, and George W. Hanson, Berry phase, Berry connection, and Chern number for a continuum bianisotropic material from a classical electromagnetics perspective, *IEEE J. Multiscale and Multiphys. Comput. Techn.* **2**, 3 (2017).
- [11] T. Ozawa, H. M. Price, A. Amo, N. Goldman, M. Hafezi, L. Lu, M. C. Rechtsman, D. Schuster, J. Simon, O. Zilberberg, and I. Carusotto, Topological photonics, *Rev. Mod. Phys.* **91**, 015006 (2019).
- [12] M. G. Silveirinha, Topological classification of Chern-type insulators by means of the photonic Green function, *Phys. Rev. B* **97**, 115146 (2018).
- [13] M. G. Silveirinha, Topological theory of non-Hermitian photonic systems, *Phys. Rev. B* **99**, 125155 (2019).
- [14] M. S. Rudner and L. S. Levitov, Topological Transition in a Non-Hermitian Quantum Walk, *Phys. Rev. Lett.* **102**, 065703 (2009).
- [15] J. M. Zeuner, M. C. Rechtsman, Y. Plotnik, Y. Lumer, S. Nolte, M. S. Rudner, M. Segev, and A. Szameit, Observation of a Topological Transition in the Bulk of a Non-Hermitian System, *Phys. Rev. Lett.* **115**, 040402 (2015).
- [16] V. Peano, M. Houde, F. Marquardt, and A. A. Clerk, Topological Quantum Fluctuations and Traveling Wave Amplifiers, *Phys. Rev. X* **6**, 041026 (2016).
- [17] D. Leykam, K. Y. Bliokh, C. Huang, Y. D. Chong, and F. Nori, Edge Modes, Degeneracies, and Topological Numbers in Non-Hermitian Systems, *Phys. Rev. Lett.* **118**, 040401 (2017).
- [18] V. M. M. Alvarez, J. E. B. Vargas, M. Berdakin, and L. E. F. F. Torres, Topological states of non-Hermitian systems, *Eur. Phys. J. Spec. Top.* **227**, 1295 (2018).
- [19] H. Shen, B. Zhen, and L. Fu, Topological Band Theory for Non-Hermitian Hamiltonians, *Phys. Rev. Lett.* **120**, 146402 (2018).
- [20] S. Yao and Z. Wang, Edge States and Topological Invariants of Non-Hermitian Systems, *Phys. Rev. Lett.* **121**, 086803 (2018).
- [21] S. Yao, F. Song, and Z. Wang, Non-Hermitian Chern Bands, *Phys. Rev. Lett.* **121**, 136802 (2018).
- [22] F. K. Kunst, E. Edvardsson, J. C. Budich, and E. J. Bergholtz, Biorthogonal Bulk-Boundary Correspondence in Non-Hermitian Systems, *Phys. Rev. Lett.* **121**, 026808 (2018).
- [23] Z. Gong, Y. Ashida, K. Kawabata, K. Takasan, S. Higashikawa, and M. Ueda, Topological Phases of Non-Hermitian Systems, *Phys. Rev. X* **8**, 031079 (2018).
- [24] K. Kawabata, K. Shiozaki, M. Ueda, and M. Sato, Symmetry and Topology in Non-Hermitian Physics, *Phys. Rev. X* **9**, 041015 (2019).
- [25] K. Y. Bliokh, D. Leykam, M. Lein, and F. Nori, Topological non-Hermitian origin of surface Maxwell waves, *Nat. Commun.* **10**, 580 (2019).
- [26] Y. Ran, Y. Zhang, and A. Vishwanath, One-dimensional topologically protected modes in topological insulators with lattice dislocations, *Nature Phys.* **5**, 298 (2009).
- [27] F.-F. Li, H.-X. Wang, Z. Xiong, Q. Lou, P. Chen, R.-X. Wu, Y. Poo, J.-H. Jiang, and S. John, Topological light-trapping on a dislocation, *Nat. Commun.* **9**, 2462 (2018).
- [28] M. Xiao, Z. Q. Zhang, and C. T. Chan, Surface Impedance and Bulk Band Geometric Phases in One-Dimensional Systems, *Phys. Rev. X* **4**, 021017 (2014).
- [29] R. Johnson and J. Moser, The rotation number for almost periodic potentials, *Commun. Math. Phys.* **84**, 403 (1982).
- [30] J. Kellendonk and I. Zois, Rotation numbers, boundary forces and gap labelling, *J. Phys. A: Math. Gen.* **38**, 3937 (2005).
- [31] S. Aubry and G. Andre, Analyticity breaking and Anderson localization in incommensurate lattices, *Ann. Isr. Phys. Soc.* **3**, 18 (1980).
- [32] X. Ni, K. Chen, M. Weiner, D. J. Apigo, C. Prodan, A. Alù, E. Prodan, and A. B. Khanikaev, Observation of Hofstadter butterfly and topological edge states in reconfigurable quasi-periodic acoustic crystals, *Comm. Phys.* **2**, 55 (2019).
- [33] A. Raman and S. Fan, Photonic Band Structure of Dispersive Metamaterials Formulated as a Hermitian Eigenvalue Problem, *Phys. Rev. Lett.* **104**, 087401 (2010).
- [34] M. G. Silveirinha, Modal expansions in dispersive material systems with application to quantum optics and topological photonics, *Advances in Mathematical Methods for Electromagnetics*, edited by P. Smith and K. Kobayashi (IET, Scitech Publishing, 2021).
- [35] L. Yuan, Q. Lin, M. Xiao, and S. Fan, Synthetic dimension in photonics, *Optica* **5**, 1396 (2018).
- [36] T. Ozawa and H. M. Price, Topological quantum matter in synthetic dimensions, *Nat. Rev. Phys.* **1**, 349 (2019).
- [37] E. Lustig, S. Weimann, Y. Plotnik, Y. Lumer, M. A. Bandres, A. Szameit, and M. Segev, Photonic topological insulator in synthetic dimensions, *Nature (London)* **567**, 356 (2019).
- [38] Y. Hatsugai, Chern Number and Edge States in the Integer Quantum Hall Effect, *Phys. Rev. Lett.* **71**, 3697 (1993).
- [39] E. Volovik, *The Universe in a Helium Droplet* (Oxford University Press, Oxford, 2003).
- [40] E. Prodan and H. Schulz-Baldes, *Bulk and Boundary Invariants for Complex Topological Insulators: From K-Theory to Physics* (Springer International Publishing, Switzerland, 2016).
- [41] M. G. Silveirinha, Bulk edge correspondence for topological photonic continua, *Phys. Rev. B* **94**, 205105 (2016).
- [42] M. G. Silveirinha, Proof of the Bulk-Edge Correspondence Through a Link Between Topological Photonics and Fluctuation-Electrodynamics, *Phys. Rev. X* **9**, 011037 (2019).
- [43] R. Bianco and R. Resta, Mapping topological order in coordinate space, *Phys. Rev. B* **84**, 241106(R) (2011).

- [44] M. D. Caio, G. Möller, N. R. Cooper, and M. J. Bhaseen, Topological marker currents in Chern insulators, *Nat. Phys.* **15**, 257 (2019).
- [45] I. E. Tamm, On the possible bound states of electrons on a crystal Surface, *Phys. Z. Sowjetunion* **1**, 733 (1932).
- [46] J. D. Joannopoulos, S. G. Johnson, J. N. Winn, and R. D. Meade, *Photonic Crystals: Molding the Flow of Light*, 2nd ed. (Princeton University Press, New York, 2008).
- [47] SIMULIA—CST Studio Suite, <https://www.3ds.com/products-services/simulia/products/cst-studio-suite/>
- [48] M. G. Silveirinha, Quantized angular momentum in topological optical systems, *Nat. Comm.* **10**, 349 (2019).
- [49] M. G. Silveirinha, Topological angular momentum and radiative heat transport in closed orbits, *Phys. Rev. B* **95**, 115103 (2017).
- [50] D. M. Pozar, *Microwave Engineering*, 4th ed. (Wiley, Hoboken, 2011).